

**COSMIC STAR FORMATION HISTORY AND DEEP X-RAY IMAGING IN THE
XMM-NEWTON AND CHANDRA ERA**

Pranab Ghosh

Department of Astronomy & Astrophysics, Tata Institute of Fundamental Research, Bombay 400 005, INDIA

ABSTRACT

I summarize X-ray diagnostic studies of cosmic star formation in terms of evolutionary schemes for X-ray binary evolution in normal galaxies with evolving star formation. Deep X-ray imaging studies by *Chandra* and *XMM-Newton* are beginning to constrain both the X-ray luminosity evolution of galaxies and the $\log N$ - $\log S$ diagnostics of the X-ray background: I discuss these in the above context, summarizing current understanding and future prospects.

Key words: galaxies: evolution – stars: formation – X-rays: galaxies – X-rays: background – binaries: close

1. INTRODUCTION

This is a brief account of the current status and future potentials of the X-ray diagnostics of the history of cosmic star-formation rate (SFR). Global SFR has undergone strong cosmological evolution: it was ~ 10 times its present value at $z \approx 1$, had a peak value ~ 10 – 100 times the present one in the redshift range $z \sim 1.5$ – 3.5 , and declined again at high z (Madau, Pozzetti & Dickinson 1998, henceforth M98; Blain, Smail, Ivison & Kneib 1999, henceforth B99a; Blain *et al.* 1999, henceforth B99b, and references therein). Details of the SFR at high redshifts are still somewhat uncertain, because much of the star formation at $2 \lesssim z \lesssim 5$ may be dust-obscured and so missed by optical surveys, but detected readily through the copious submillimeter emission from the dust heated by star formation.

The X-ray emission of a normal galaxy (*i.e.*, one without an active nucleus) is believed to be dominated by the integrated emission of the galaxy’s X-ray binary population: this statement may be somewhat dependent on the X-ray energy band (see Sec. 5), but current understanding does suggest that, in the canonical 2–10 keV X-ray band, the statement is valid for most normal galaxies. I summarize in this paper recent studies made in collaboration with N. White, A. Ptak, and R. Griffiths (White & Ghosh 1998, henceforth WG98; Ghosh & White 2001, henceforth GW01; Ptak *et al.* 2001, henceforth Ptak01) on the basic imprints of an evolving SFR on the evolution of X-ray binary populations of galaxies, on the general consequences

of these studies for deep X-ray imaging of galaxy fields by *Chandra* and *XMM-Newton*, and on the first, specific results that have emerged so far on the X-ray luminosity evolution in the Hubble Deep Field (HDF), and on the $\log N$ - $\log S$ diagnostics of the X-ray background. First results of Brandt *et al.* (2001, henceforth Bran01) from the ~ 0.5 Ms *Chandra* exposure of HDF North (HDF-N) suggest an evolution of the X-ray luminosities, L_X , of bright spirals from the Local Universe to $z \approx 0.5$, which I compare with the GW01 predictions from current SFR models: I also discuss the roles of global and individual SFR histories in this context. Fluctuation analyses of the ~ 1 Ms *Chandra* exposure of (HDF-N) suggest (Miyaji & Griffiths 2002, henceforth MG02) that the $\log N$ - $\log S$ plot in the soft X-ray band continues to rise at low ($S \sim 10^{-16}$ – 10^{-17} erg cm $^{-2}$ s $^{-1}$) fluxes, indicating that the X-ray background at these fluxes is possibly dominated by a new population of faint X-ray sources rather than the canonical integrated AGN population (Gilli *et al.* 2001, henceforth GSH), whose contribution shows a cosmological flattening at these fluxes, and so lies much below the observational values suggested by MG02: in view of the Ptak01 predictions which I discuss, it is plausible that this additional population is, in fact, that of normal galaxies showing the signature of their SFR histories through X-ray emission.

2. SFR PROFILES AND X-RAY LUMINOSITY EVOLUTION

In the approach of WG98 and GW01, the total X-ray output of a normal galaxy is modeled as the sum of those of its high-mass X-ray binaries (HMXB) and low-mass X-ray binaries (LMXB), the evolution of each species “ i ” being described by a timescale τ_i . The effects of the dependence of τ_i on the binary period and other parameters are studied by running the evolutionary scheme over ranges of likely values of τ_i given in the literature. The evolution of the HMXB population in response to an evolving star-formation rate SFR(t) is given by

$$\frac{\partial n_{\text{HMXB}}(t)}{\partial t} = \alpha_h \text{SFR}(t) - \frac{n_{\text{HMXB}}(t)}{\tau_{\text{HMXB}}}, \quad (1)$$

where n_{HMXB} is the number density of HMXBs in the galaxy, and τ_{HMXB} is the HMXB evolution timescale. α_h is the rate of formation of HMXBs per unit SFR, given approximately by $\alpha_h = \frac{1}{2} f_{\text{binary}} f_{\text{prim}}^h f_{\text{SN}}^h$, where f_{binary} is the fraction of all stars in binaries, f_{prim}^h is that fraction of primordial binaries which has the correct range of

stellar masses and orbital periods for producing HMXBs (van den Heuvel 1992, henceforth vdH92), and $f_{\text{SN}}^h \approx 1$ is that fraction of massive binaries which survives the first supernova. In these calculations, a representative value $\tau_{\text{HMXB}} \sim 5 \times 10^6$ yr is adopted according to current evolutionary models. Note that τ_{HMXB} includes both (a) the time taken ($\sim 4 - 6 \times 10^6$ yr) by the massive companion of the neutron star to evolve from the instant of the neutron-star-producing supernova to the instant when the “standard” HMXB phase begins, and, (b) the (much shorter) duration ($\sim 2.5 \times 10^4$ yr) of this HMXB phase (vdH92 and references therein).

Of the two mechanisms of LMXB production generally envisaged, *viz.*, (a) production in cores of globular clusters due to tidal capture, and, (b) general production by evolution of primordial binaries, I describe here only the latter one (which must be the dominant mechanism at least for spiral galaxies, since globular-cluster LMXB populations of such galaxies can account only for relatively small fractions of their total X-ray luminosities), deferring the former to Sec. 5. LMXB evolution from primordial binaries has two stages (WG98) after the supernova produces a post-supernova binary (PSNB) containing the neutron star. First, the PSNB evolves on a timescale τ_{PSNB} due to nuclear evolution of the neutron star’s low-mass companion and/or decay of binary orbit due to gravitational radiation and magnetic braking, until the companion comes into Roche lobe contact and the LMXB turns on. Subsequently, the LMXB evolves on a timescale τ_{LMXB} . Since τ_{PSNB} and τ_{LMXB} are comparable in general, the two stages are described separately (WG98) by:

$$\frac{\partial n_{\text{PSNB}}(t)}{\partial t} = \alpha_l \text{SFR}(t) - \frac{n_{\text{PSNB}}(t)}{\tau_{\text{PSNB}}}, \quad (2)$$

$$\frac{\partial n_{\text{LMXB}}(t)}{\partial t} = \frac{n_{\text{PSNB}}(t)}{\tau_{\text{PSNB}}} - \frac{n_{\text{LMXB}}(t)}{\tau_{\text{LMXB}}}, \quad (3)$$

Here, n_{PSNB} and n_{LMXB} are the respective number densities of PSNB and LMXB in the galaxy, and α_l is the rate of formation of LMXB per unit SFR, given approximately by $\alpha_l = \frac{1}{2} f_{\text{binary}} f_{\text{prim}}^l f_{\text{SN}}^l$, the individual factors having meanings closely analogous to those for HMXBs (see GW01).

Evolution is displayed in terms of the redshift z , which is related to the cosmic time t by $t_9 = 13(z+1)^{-3/2}$, where t_9 is t in units of 10^9 yr, and a value of $H_0 = 50 \text{ km s}^{-1} \text{ Mpc}^{-1}$ has been used¹. I consider the suite of current SFR models detailed in Table 1 to cover a plausible range, using the parameterization of B99a,b. Models of the “peak” class have the form:

$$\text{SFR}_{\text{peak}}(z) = 2 \left(1 + \exp \frac{z}{z_{\text{max}}} \right)^{-1} (1+z)^{p + \frac{1}{2z_{\text{max}}}}, \quad (4)$$

¹ For ease of comparison with WG98, M98, and GW01, I use here a Friedman cosmology with $q_0 = 1/2$. Other values of the Hubble constant lead to a straightforward scaling: for $H_0 = 70 \text{ km s}^{-1} \text{ Mpc}^{-1}$, for example, $t_9 \approx 10(z+1)^{-3/2}$, so that the results remain unchanged if all timescales are shortened by a factor of 1.3.

while those of the “anvil” class have the form:

$$\text{SFR}_{\text{anvil}}(z) = \begin{cases} (1+z)^p, & z \leq z_{\text{max}}, \\ (1+z_{\text{max}})^p, & z > z_{\text{max}}. \end{cases} \quad (5)$$

Table 1. Star Formation Rate (SFR) Profiles

Model	z_{max}	p	Comments
Peak-M	0.39	4.6	Madau profile
Hierarchical	0.73	4.8	Hierarchical Clustering
Anvil-10	1.49	3.8	Monolithic Models
Peak-G	0.63	3.9	Peak part of composite “Gaussian” Model
Gaussian	N/A	N/A	Gaussian starburst added at high z

These functional forms are convenient since they have a convenient low- z limit, $\text{SFR}(z) \propto (1+z)^p$, where all SFR profiles must agree with the optical/UV data (M98), and since the model parameters can be manipulated to mimic a wide range of star-formation histories (B99b). Peak-class profiles are useful for describing (a) SFRs determined from optical/UV observations, *i.e.*, Madau-type (M98) profiles, called “Peak-M” in Table 1, and, (b) more general SFRs with enhanced star formation at high z , an example of which is the “hierarchical” model of B99b, wherein the submillimeter emission is associated with galaxy mergers in an hierarchical clustering model. Anvil-class profiles are useful for describing the results of “monolithic” models. The “Gaussian” model (B99a,b) is an attempt at giving a good account of the SFR at both low and high z by making a composite of the Peak-G model (see Table 1) and a Gaussian starburst at a high redshift z_p , *i.e.*, a component

$$\text{SFR}_{\text{Gauss}}(z) = \Theta \exp \left\{ -\frac{[t(z) - t(z_p)]^2}{2\sigma^2} \right\}. \quad (6)$$

Based on the *IRAS* luminosity function, this component is devised to account for the high- z data, particularly the submillimeter observations (B99a). For its parameters (see Table 1), I have used the revised values given in B99b (see GW01). In all models described here, no galaxies exist for sufficiently large redshifts, $z > 10$. Figure 1 shows the prompt evolution of HMXBs and the slow evolution of LMXBs, and the evolution of the total X-ray binary population, where the two components have been so weighted as to represent the total X-ray emission from the galaxy. The HMXB profile closely follows the SFR profile because τ_{HMXB} is small compared to the SFR evolution timescale. By contrast, the LMXB profile has a significant lag behind the SFR profile because τ_{PSNB} and τ_{LMXB} are comparable to SFR evolution timescale: the LMXB profile generally peaks at redshifts $\sim 1 - 3$ later than the HMXB profile — a characteristic signature of SFR evolution (WG98). Effects of both (a) varying the evolutionary timescales for fixed

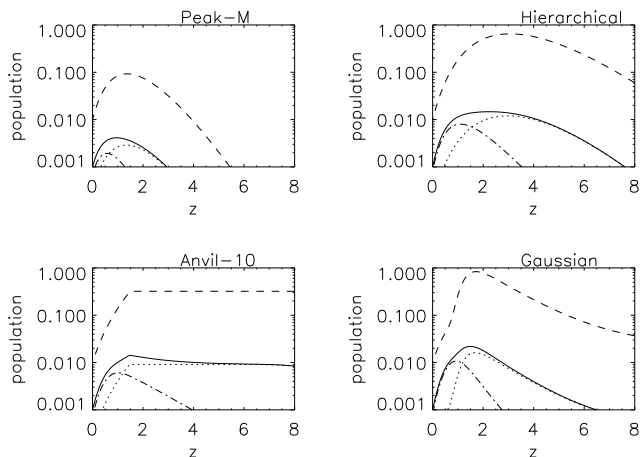


Figure 1. Evolution of HMXB population (dotted line), LMXB population (dash-dotted line), and the total X-ray luminosity L_X (solid line) of a galaxy with various SFR profiles (dashed line), from GW01. The effects of SFR variation are shown by keeping the evolutionary timescales fixed at $\tau_{\text{PSNB}} = 1.9$ Gyr and $\tau_{\text{LMXB}} = 1.0$ Gyr for all cases, and choosing various SFR profiles from Table 1. Each panel is labeled by the name of its SFR profile.

SFR profiles, and, (b) varying the SFR profile for fixed evolutionary timescales have been studied: see GW01 for details. I display the latter variation in Figure 1 to emphasize that, since, for sufficiently *slow* LMXB evolution, the galaxy’s X-ray emission is dominated by LMXBs at low redshifts ($0 \lesssim z \lesssim 1$), and by HMXBs at high redshifts, the total L_X -profile is strongly influenced at high redshifts by the SFR profile. Thus, determination of the L_X -profile even upto moderate redshifts may put interesting constraints on the SFR, making this an *independent* X-ray probe of cosmic star-formation history.

From their stacking analysis (see Bran01 and references therein for an exposition of the technique), Bran01 estimate that the average X-ray luminosity of the bright spiral galaxies at an average redshift $z \approx 0.5$ used in their study is about a factor of 3 higher than that in the local Universe. This observed evolution, $L_X(0.5)/L_X(0.0) \sim 3$, can be compared with the theoretical results in Table 2. The degree of evolution from $z = 0$ to $z = 0.5$ – 1.0 increases from Madau-type profiles to those with additional star formation at high redshifts, the numbers for the Peak-M profile being in best agreement with Bran01.

3. GLOBAL AND INDIVIDUAL SFRS

A new development in SFR research in the last three years has been the study of star-formation histories of individual galaxies and various galaxy-types. SFR profiles of individual galaxies, ranging from those in the Local Group to those in the HDF at redshifts $0.4 \lesssim z \lesssim 1$, have been

Table 2. Evolution of X-ray Luminosity L_X

Model	τ_{PSNB}	τ_{LMXB}	$\frac{L_X(0.5)}{L_X(0.0)}$	$\frac{L_X(1.0)}{L_X(0.0)}$
Peak-M	1.9	0.1	3.9	5.4
Peak-M	0.9	0.5	4.6	6.8
Peak-M	1.9	1.0	3.4	4.1
Hierarchical	1.9	1.0	6.2	11.3
Anvil-10	1.9	1.0	5.4	10.1
Gaussian	1.9	1.0	7.5	16.0

inferred, using a variety of techniques. For various galaxy-types, models of spectrophotometric evolution, which use the synthesis code *Pégase* and are constrained by deep galaxy counts, have been developed (Rocca-Volmerange and Fioc 2000, henceforth RF00), leading to a model SFR profile for each type. In the light of these developments, let me now suggest what may be the true significance of the Bran01 results discussed above.

Bran01 used bright spirals for their stacking analysis. RF00 have shown that the model SFR profile for such (Sa-Sbc) spirals rises roughly in a Madau fashion from $z = 0$ to $z \approx 1$ (which these authors ascribe to a bias in the original sample used to construct the Madau profile towards bright spirals), and thereafter flattens to a roughly constant value ~ 12 times that at $z = 0$, falling again at $z \gtrsim 7$. In the range $0 < z \lesssim 7$, this profile can be roughly represented by an anvil-type profile (see Sec. 2), with the parameter z_{max} as given in Table 1, and the parameter $p \approx 2.7$. For such a profile with the timescales $\tau_{\text{PSNB}} = 1.9$ Gyr, $\tau_{\text{LMXB}} = 1.0$ Gyr, as in Figure 1, the GW01 evolutionary scheme gives $L_X(0.5)/L_X(0.0) = 3.3$, and $L_X(1.0)/L_X(0.0) = 5.4$, in good agreement with both the Bran01 results and the Peak-M results given in Table 2. It is now easy to see to see why the Peak-M profile would appear to give a good account of the Bran01 results. In effect, the Bran01 analysis may be probing the SFR profile of *only* the bright spirals in HDF-N, and the fact that the Peak-M profile is consistent with the Bran01 results does *not* imply that the global SFR necessarily follows the Peak-M profile.

4. $\log N$ – $\log S$ DIAGNOSTICS: X-RAY BACKGROUND

Based on the results of Sec. 2, Ptak01 calculated the X-ray flux distributions and source count ($\log N$ – $\log S$) plots expected for HDF-N. Figure 2 shows the Ptak01 plot in the soft (0.5–2.0 keV) X-ray band, which has proved to be a valuable diagnostic of current population synthesis models of the X-ray background, as I now summarize. Hasinger (2002, henceforth H02) reminds us that the cosmic X-ray background has, in this *Chandra* and *XMM-Newton* era of deep X-ray surveys, been largely resolved into contributions from individual sources, the resolved fraction being $\gtrsim 90\%$ in the soft (0.5–2.0 keV) band, and similar

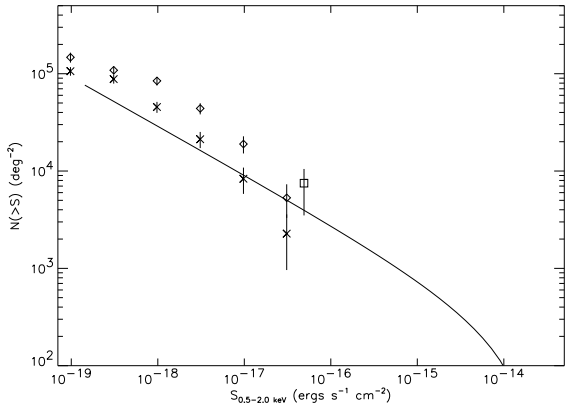


Figure 2. $\log N$ - $\log S$ plot in the soft (0.5 – 2.0 keV) band for HDF-N, from Ptak01. The diamonds correspond to the Gaussian SFR profile described in Sec. 2, and the crosses to the Peak-M profile. Note that an interpolation through the former points is represented by a dashed line in Fig.2 of MG02 and Fig.2 (bottom) of H02, and that through the latter points by a dotted line. The solid line here is the double power law fit of Tozzi et al. to the Chandra observations of HDF South.

in the harder (2–10 keV) band. The long-standing belief that these sources are predominantly active galactic nuclei (AGN), both unobscured and obscured (the so-called QSO-2s), was supported by the (now completed) optical identification programme which followed up the ROSAT deep survey, since it found the counterparts to be predominantly AGN. Ongoing optical identifications of the deepest *Chandra* and *XMM-Newton* fields are still far from complete. AGN population-synthesis models of the X-ray background are currently very useful and popular: these have been developed to a degree of sophistication and detail (see GSH, which has references to earlier models) sufficient for extracting information about AGN population properties. The recent, ultradeep (~ 1 Ms) observations of both HDF-N and the Chandra Deep Field South (CDFS) have led to $\log N$ - $\log S$ plots in the soft (0.5–2.0 keV) X-ray band which go down to fluxes $S \sim 5 \times 10^{-17}$ erg cm $^{-2}$ s $^{-1}$: these are fitted well by the GSH models, which show a clear cosmological flattening at fluxes below the above limit (H02; MG02).

Fluctuation analysis is a powerful tool for constraining the source counts below source detection limit (see MG02 and references therein for an exposition of the method), which has been successfully tested on data from previous X-ray missions. Its recent application by MG02 to the 1 Ms observation of HDF-N has yielded the remarkable result that the constraints so obtained on the soft-band $\log N$ - $\log S$ plot suggest that the extension of the plot down to fluxes $S \sim 7 \times 10^{-18}$ erg cm $^{-2}$ s $^{-1}$ continues to rise as at higher fluxes, showing no signs of the cosmological flattening characteristic of the GSH models (MG02;

H02). The most obvious interpretation is that, while the AGN contribution, as modelled by GSH, begins to saturate at these fluxes, a new population of faint sources begins to dominate. The fact that the extension of the $\log N$ - $\log S$ plot, as inferred from the fluctuation-analysis constraints of MG02, agree well with that shown in the above Ptak01 plot (since the figure showing this appears twice in these proceedings, Fig.2 in MG02 and Fig.2 (bottom) in H02, I do not repeat it here), particularly for the Gaussian SFR profile, therefore opens the exciting possibility that first signatures of cosmic star formation in the soft X-ray band $\log N$ - $\log S$ plots are revealing themselves.

5. FUTURE PROSPECTS

Even in this *Chandra* and *XMM-Newton* era, truly new results on L_X -evolution and SFR signature have been possible so far only by going below the source detection limit with special techniques like stacking and fluctuation analysis. These are suggestive indications, which must be confirmed with source detection at lower fluxes, first with longer exposures with *Chandra* and *XMM-Newton*, and then with the next generation of satellites like *Constellation-X* and *XEUS*. On the theoretical side, the evolutionary scheme must be generalized to include several additional effects, *e.g.*, (a) in the soft X-ray band, the output of a normal galaxy may have very significant contributions from supernova remnants (G. Hasinger, personal communication), and, (b) tidal capture creation of LMXBs in globular clusters may be the dominant production mechanism in certain galaxy-types. Inclusion of these effects presents no difficulties of principle, and is now under way: the results will be described elsewhere.

REFERENCES

- Blain, A. W., Smail, I., Ivison, R. J. & Kneib, J.-P. 1999, MNRAS 302, 632 (B99a)
 Blain, A. W., Jameson, A., Smail, I., Longair, M. S., Kneib, J.-P. & Ivison, R. J. 1999, MNRAS 309, 715 (B99b)
 Brandt, W. N. et al., 2001, AJ 122, 1 [astro-ph/0102411] (Bran01)
 Ghosh, P. & White, N. 2001, ApJ 559, L97 (GW01)
 Gilli, R., Salvati, M., & Hasinger, G. 2001, A&A 366, 407 (GSH)
 Hasinger, G. 2002, these proceedings [astro-ph/0202430] (H02)
 Madau, P., Pozzetti, L., & Dickinson, M. 1998, MNRAS 498, 106 (M98)
 Miyaji, T. & Griffiths, R. 2002, these proceedings [astro-ph/0202048] (MG02)
 Ptak, A., Griffiths, R., White, N. & Ghosh, P. 2001, ApJ 559, L91 (Ptak01)
 Rocca-Volmerange, B. & Fioc, M. 2000, in Toward A New Millennium in Galaxy Morphology, ed. D. L. Block, I. Puerari, A. Stockton & D. Ferreira, Kluwer: Dordrecht [astro-ph/0001398] (RF00)
 White, N. & Ghosh, P. 1998, ApJ 504, L31 (WG98)

van den Heuvel, E. P. J. 1992, in X-ray Binaries and Recycled Pulsars, ed. E. P. J. van den Heuvel and S. A. Rappaport, Kluwer: Dordrecht, p.233 (vdH92)